	Uesato S, Mochizuki H			
Less constraint, non-invasive rehabilitation system for patients with neurological disease using functional near infrared spectroscopy(fNIRS).	Mihara M, Mochizuki H.	17th annual meeting of American society for experimental neurotherapeutics.	2015年2月	国外

2．学会誌・雑誌等における論文掲載

掲載した論文（発表題目）	発表者氏名	発表した場所（学会誌・雑誌等名）	発表した時期	国内・外の別
Official Japanese Version of the Movement Disorder Society-Unified Parkinson's Disease Rating Scale: validation against the original English version.	Kashihara K, Kondo T, Mizuno Y, Kikuchi S, Kuno S, Hasegawa K, Hattori N, Mochizuki H, Mori H, Murata M, Nomoto M, Takahashi R, Takeda A, Tsuboi Y, Ugawa Y, Yamanmoto M, Yokochi F, Yoshii F, Stebbins GT, Tilley BC, Luo S, Wang	Mov Disord Clin Pract (Hoboken).	2014 Sep	国外

	L, LaPelle NR, Goetz CG:MDS-UPDRS Japanese Validation Study Group.			
神経リハビリテーションにおける近赤外分光法の応用	三原雅史	Jpn J Rehabil Med	2014　10月	国内

機関名：大阪大学大学院医学研究科　放射線医学講座

１．学会等における口頭・ポスター発表

発表した成果（発表題目、口頭・ポスター発表の別）	発表者氏名	発表した場所（学会等名）	発表した時期	国内・外の別
口頭発表				
４D-FLOW MRIを用いた脳動脈瘤内における血流動態の可視化	渡邉嘉之、國富裕樹、田中壽、塚部明大、有澤亜津子、松尾千聡、藤中俊之、富山憲幸	第42回日本磁気共鳴医学会	2014年9月	国内
ポスター発表				
なし				

２．学会誌・雑誌等における論文掲載

掲載した論文（発表題目）	発表者氏名	発表した場所（学会誌・雑誌等名）	発表した時期	国内・外の別
Neuromelanin magnetic resonance imaging reveals increased dopaminergic neuron activity in the substantia	Watanabe Y, Tanaka H, Tsukabe A, Kunitomi Y, Nishizawa M,	PLOS ONE	2014 Aug	国外

nigra of patients with schizophrenia.	Hashimoto R, Yamamori H, Fujimoto M, Fukunaga M, Tomiyama N.			
Model-based iterative reconstruction for detection of subtle hypoattenuation in early cerebral infarction: a phantom study.	Nishizawa M, Tanaka H,?Watanabe Y, Kunitomi Y, Tsukabe A, Tomiyama N.	Jpn J Radiol.	2014 Nov	国内
Abnormal Corpus Callosum Connectivity, ocio-communicative Deficits, and Motor Deficits in Children with Autism Spectrum Disorder: A Diffusion Tensor Imaging Study.	Hanaie R, Mohri I, Kagitani-Shimono K, Tachibana M, Matsuzaki J, Watanabe Y, Fujita N, Taniike M.	J Autism Dev Disord.	2014 Sep	国外
Genetic and environmental influences on motor function: a magnetoencephalographic study of twins.	Araki T, Hirata M, Sugata H,X Yanagisawa H, Onishi M ,Watanabe Y, Omura K, Honda C, Hayakawa K, Yorifuji S.	Frontiers in Human Neuroscience	2014 June	国外
Cerebral Aneurysm Pulsation: Do Iterative Reconstruction Methods Improve Measurement Accuracy in Vivo?	Illies T, S t ring D, Kinoshita M, Fujinaka T, Bester M, Fiehler J, Tomiyama N, Watanabe Y.	AJNR Am J Neuroradiol.	2014 Nov	国外
Genetic risk variants of schizophrenia associated with left superior	Ohi K, Hashimoto R, Ikeda M, Yamashita F,	Cortex.	2014 Sep	国外

temporal gyrus volume.	Fukunaga M, Nemoto K, Ohnishi T, Yamamori H, Yasuda Y, Fujimoto M, Umeda-Yano S,?Watanabe Y, Iwata N, Weinberger DR, Takeda M.			
Prevalence and diagnostic performance of computed tomography angiography spot sign for intracerebral hematoma expansion depend on scan timing.	Tsukabe A, Watanabe Y, Tanaka H, Kunitomi Y, Nishizawa M, Arisawa A, Yoshiya K, Shimazu T, Tomiyama N.	Neuroradiology.	2014 Dec	国外
Pituitary-targeted dynamic contrast-enhanced multi-slice computed tomography for detecting magnetic resonance imaging-occult functional pituitary microadenoma.	Kinoshita M, Tanaka H, Arita H, Goto MY, Oshino S, Watanabe Y, Yoshimine T, Saitoh Y.	AJNR	2015 Jan.	国外

機関名：社会医療法人大道会　森之宮病院

1．学会等における口頭・ポスター発表

発表した成果(発表題目、口頭・ポスター発表の別)	発表者氏名	発表した場所（学会等名）	発表した時期	国内・外の別
口頭発表				
回復期リハビリテーショ	藤本宏明,	第37回日本リハビリ	2014年9月	国内

ン病院入院中、繰り返す嘔吐を契機にSMA（Superior mesenteric artery syndrome;上腸間膜動脈）症候群と診断した一例.	畠中めぐみ, 跡地春仁, 長廻倫子, 吉岡知美, 河野悌二, 服部憲明, 矢倉一, 宮井一郎.	テーション医学会近畿地方会		
ポスター発表				
ゲイトジャッジシステムを用いた歩行カンファレンスの有効性	矢倉一,宮井一郎,服部憲明,畠中めぐみ,河野悌司,藤本宏明,吉岡知美,乙宗宏範,川口敏和	第51回日本リハビリテーション医学会学術集会	2014年6月	国内
NIRSを用いたニューロフィードバックによる脳卒中後上肢麻痺改善効果の検討	藤本宏明,三原雅史,服部憲明,畠中めぐみ,矢倉一,河野悌司,河原田倫子,吉岡知美,乙宗宏範,宮井一郎	第51回日本リハビリテーション医学会学術集会	2014年6月	国内
Large-scale EEG phase synchrony associated with functional recovery after ischemic stroke	Uno Y, Kawano T,Hattori N, Hatakenaka M,Miyai I, Kitajo K	Organization for Human Brain Mapping 2014 Annual Meeting	2014年6月	国外
NIRSを用いたニューロフィードバックによる脳卒中後上肢麻痺改善効果の検討	藤本宏明,三原雅史,服部憲明,畠中めぐみ,矢倉一,	第17回日本光脳機能イメージング学会	2014年7月	国内

	河野悌司,吉岡知美,長廻倫子,望月秀樹,宮井一郎			
Facilitating supplementary motor area using near-infrared spectroscopy mediated neurofeedback improves postural stability but not hand dexterity	Fujimoto H, Mihara M, Hattori N, Hatakenaka M, Yagura H, Kawano T, Otomune H, Miyai I, Mochizuki H	第44回北米神経学会	2014年11月	国外
Phase synchrony of resting state electroencephalography in ischemic stroke:I. Distinct effects of band frequency on various aspects of functional outcome	Kawano T,Hattori N, Uno Y, Kitajyo K, Hatakenaka M,Yagura H,Fujimoto H,Yoshioka T,Nagasako M, Otomune H,Miyai I.	第44回北米神経学会	2014年11月	国外
Facilitating supplementary motor area using near-infrared spectroscopy mediated neurofeedback improves postural stability but not hand dexterity	Fujimoto H, Mihara M, Hattori N, Hatakenaka M, Yagura H, Kawano T, Otomune H, Miyai I, Mochizuki H	2014 American Society of Neurorehabilitation Annual Meeting	2014年11月	国外

脳卒中患者に対する近赤外分光法(NIRS)を用いたニューロフィードバックによる姿勢バランス能力改善効果の予備的検討.	藤本宏明,三原雅史,矢倉一,畠中めぐみ,服部憲明,河野悌司,望月秀樹,宮井一郎	第6回日本ニューロリハビリテーション学会学術集会	2015年2月	国内
虚血性脳卒中患者における半球間脳波位相同期とADL指標に関する報告	河野悌司,服部憲明,宇野裕,北城圭一,畠中めぐみ,矢倉一,藤本宏明,乙宗宏範,宮井一郎	第6回日本ニューロリハビリテーション学会学術集会	2015年2月	国内

2．学会誌・雑誌等における論文掲載

掲載した論文（発表題目）	発表者氏名	発表した場所（学会誌・雑誌等名）	発表した時期	国内・外の別
なし				

Neuromelanin Magnetic Resonance Imaging Reveals Increased Dopaminergic Neuron Activity in the Substantia Nigra of Patients with Schizophrenia

Yoshiyuki Watanabe[1*], Hisashi Tanaka[1], Akio Tsukabe[1], Yuki Kunitomi[1], Mitsuo Nishizawa[1], Ryota Hashimoto[2,4], Hidenaga Yamamori[4], Michiko Fujimoto[4], Masaki Fukunaga[3], Noriyuki Tomiyama[1]

1 Diagnostic and Interventional Radiology, Osaka University Graduate School of Medicine, Suita, Japan, **2** Research Center for Children's Mental Development, United Graduate School of Child Development, Osaka University, Suita, Japan, **3** Departments of Biofunctional Imaging and Immunology, Frontier Research Center, Osaka University, Suita, Japan, **4** Department of Psychiatry, Osaka University Graduate School of Medicine, Suita, Japan

Abstract

Purpose: The dopamine hypothesis suggests that excessive dopamine release results in the symptoms of schizophrenia. The purpose of this study was to elucidate the dopaminergic and noradrenergic neurons using 3-T neuromelanin magnetic resonance imaging (MRI) in patients with schizophrenia and healthy control subjects.

Methods: We prospectively examined 52 patients with schizophrenia (M: F = 27:25, mean age, 35 years) and age- and sex-matched healthy controls. Using a 3T MRI unit, we obtained oblique T1-weighted axial images perpendicular to the brainstem. We measured the signal intensity and area for the substantia nigra (SNc), midbrain tegmentum, locus ceruleus (LC), and pons. We then calculated the contrast ratios (CR) for the SNc (CR_{SN}) and LC (CR_{LC}), which were compared between patients and healthy controls using unpaired *t*-tests.

Results: The SNc and LC were readily identified in both patients and healthy controls as areas with high signal intensities in the posterior part of the cerebral peduncle and in the upper pontine tegmentum. The CR_{SN} values in patients were significantly higher than those in healthy controls (10.89±2.37 vs. 9.6±2.36, $p<0.01$). We observed no difference in the CR_{LC} values between the patients and healthy controls (14.21±3.5 vs. 13.44±3.37, $p = 0.25$). Furthermore, there was no difference in area of the SNc and LC between schizophrenia patients and controls.

Conclusions: Neuromelanin MRI might reveal increased signal intensity in the SNc of patients with schizophrenia. Our results indicate the presence of excessive dopamine products in the SNc of these patients.

Citation: Watanabe Y, Tanaka H, Tsukabe A, Kunitomi Y, Nishizawa M, et al. (2014) Neuromelanin Magnetic Resonance Imaging Reveals Increased Dopaminergic Neuron Activity in the Substantia Nigra of Patients with Schizophrenia. PLoS ONE 9(8): e104619. doi:10.1371/journal.pone.0104619

Editor: Juan Zhou, Duke-NUS Graduate Medical School, Singapore

Received February 14, 2014; **Accepted** July 15, 2014; **Published** August 11, 2014

Funding: This work was supported by research grants from KAKENHI, 22390225-Grant-in-Aid for Scientific Research (B), 23659565-Grant-in-Aid for Challenging Exploratory Research and Grant-in-Aid for Scientific Research on Innovative Areas (Comprehensive Brain Science Network) from the Japanese Ministry of Education, Culture, Sports, Science and Technology (MEXT), and the Japan Foundation for Neuroscience and Mental Health. The funders had no role in study design, data collection and analysis, decision to publish, or preparation of the manuscript.

Competing Interests: One of the co-authors, Ryota Hashimoto, United Graduate School of Child Development, Osaka University, is an editor of PLOS ONE. This does not alter the authors' adherence to PLOS ONE policies on sharing data and materials.

* Email: watanabe@radiol.med.osaka-u.ac.jp

Introduction

Dopamine dysfunction plays an important role in the pathogenesis of schizophrenia [1]. The dopamine hypothesis suggests that excessive dopamine release results in symptoms of schizophrenia. *In vivo* positron emission tomography (PET) studies in patients with schizophrenia have indicated an increased baseline occupancy of D2 receptors by dopamine [2] and an increased capacity for striatal dopamine synthesis [3]. However, PET is not widely available, and its use in research is limited because of its high production costs. Further, the short half-life of ^{11}C radiopharmaceuticals restricts their use to only institutions having a cyclotron on-site.

Neuromelanin is a byproduct of the synthesis of monoamine neurotransmitters, such as noradrenalin and dopamine, and is mainly distributed within neurons of the substantia nigra (SNc) or locus ceruleus (LC) [4]. Neuromelanin has a T1-shortening effect, which was a similar characteristic of the cutaneous melanin. High-field magnetic resonance imaging (MRI), such as 3 T, is very sensitive to tissue T1 relaxation and are able to depict tissue containing neuromelanin in (SNc) or (LC) [5]. There are many previous reports which showed the signal decrease in Parkinson's disease using neuromelanin MRI [4,6–10], but there are only two reports using this technique for schizophrenia [11,12].

The purpose of this study was to use 3T neuromelanin MRI for examining dopaminergic and noradrenergic nuclei in patients with schizophrenia and healthy controls.

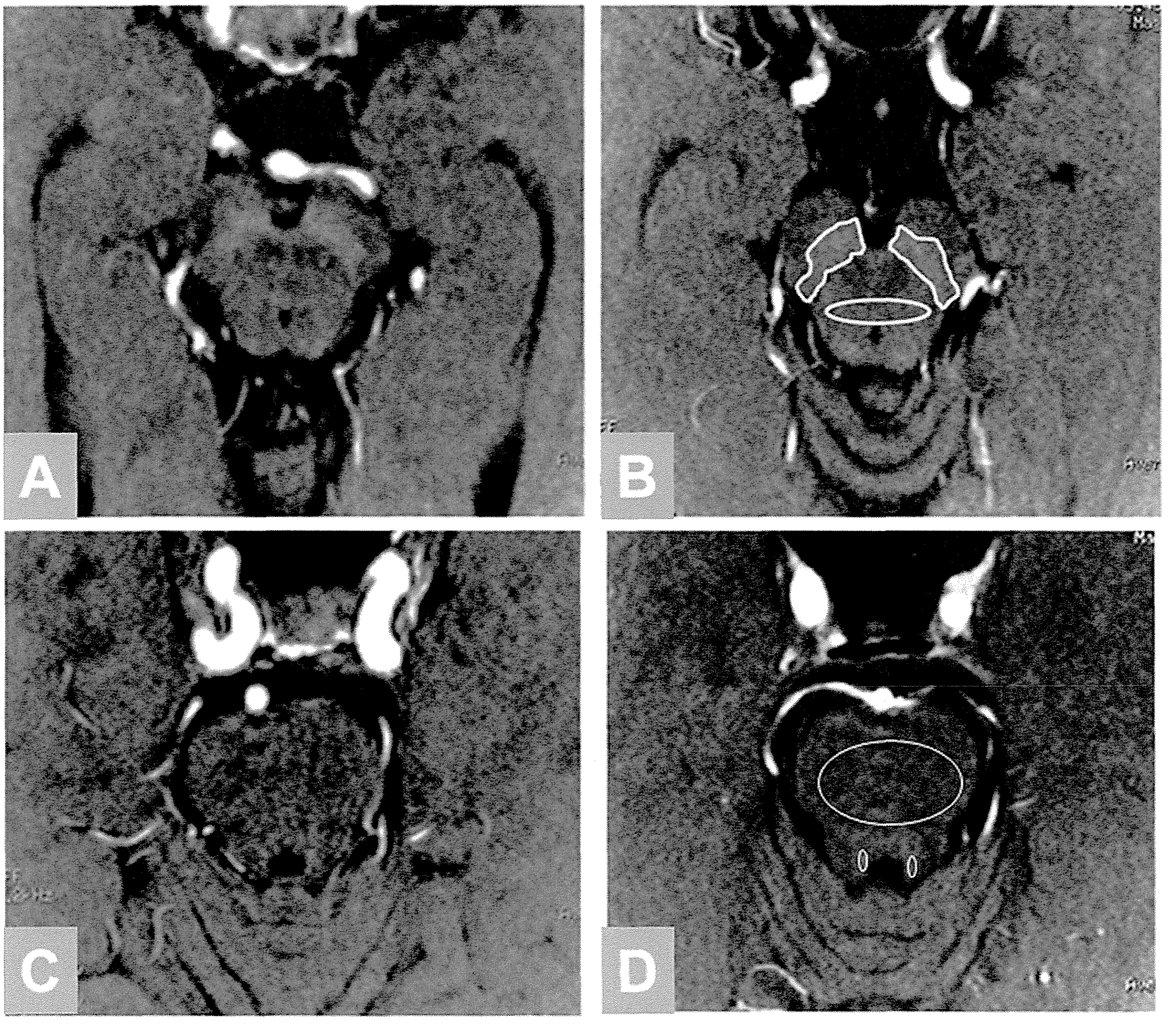

Figure 1. Neuromelanin imaging in the midbrain. A, C: 30-year-old male with schizophrenia, $CR_{SN} = 12.9$, $CR_{LC} = 10.7$; B, D: 26-year-old female healthy control, $CR_{SN} = 6.2$, $CR_{LC} = 7.6$ Demonstrating a region of interest drawn around the substantia nigra and midbrain tegmentum side on Figure 1B and locus ceruleus on Figure 1D.
doi:10.1371/journal.pone.0104619.g001

Materials and Methods

Subjects

From April to November 2012, we prospectively examined 63 consecutive patients with schizophrenia who met the *Diagnostic and Statistical Manual of Mental Disorders, 4th Edition*, (DSM-IV) diagnostic criteria using 3T-MRI. Eleven patients were excluded because of motion artifacts (6 patients) and equipment failure (5 patients). Therefore, 52 patients (M: F = 27:25; mean age = 35 years; range = 17–69 years) were included in the analysis. In addition, we obtained MRI data from age- and sex-matched healthy controls. Controls were recruited from the community through local advertisements at Osaka University. An institutional review board approved this study, and written informed consent was obtained from all subjects before their participation. We used the Japanese version of the Positive and Negative Symptom Scale (PANSS) [13] to assess patient symptoms and their severity scores. We administered the Japanese version of Wechsler Adult Intelligence Scale III [14] to determine the full scale intelligence quotient (IQ). Premorbid IQ was estimated using the Japanese Adult Reading Test [15,16].

This study was performed in accordance with the World Medical Association's Declaration of Helsinki and approved by the local institutional review board (2013-423, Osaka University Ethics Committee). Written informed consent was obtained by all subjects. If the subjects were under 20 years old, written informed consent was obtained from both minors and guardians. If the patients with schizophrenia were difficult condition to accept consent by theirself, these patients were not included in this study.

Imaging protocol

Using a 3T MRI unit (Signa Excite HDxt, GE healthcare, Milwaukee, Wisconsin), we obtained oblique T1-weighted oblique axial images perpendicular to the brainstem. The T1-weighted

Table 1. Clinical characteristics of patients with schizophrenia and healthy controls.

	Schizophrenia	Control		Schizophrenia	Control	
	all n = 52	**all n = 52**	**p value**	**<30 year n = 24**	**<30 year n = 29**	**p value**
Age	35.1 (13.3)	34.6 (13.7)	0.89	23.8 (4.1)	23.0 (2.3)	0.34
Sex (male:female)	27:25	27:25		11:13	16:13	
Year of education	13.4 (2.5)	15.4 (2.1)	<.001	13.0 (2.7)	15.6 (1.6)	<.001
Smoking (%)	16 (31%)	4 (7.7%)	<.001	6 (25%)	1 (3.4%)	<.001
Estimated premorbid IQ.	102.0 (10.9)	109.7 (7.3)	<.001	102.0 (11.2)	111.3 (5.0)	<.001
Full scale IQ	87.0 (20.9)	113.8 (14.1)	<.001	87.8 (20.4)	118.4 (11.4)	<.001
Age of onset	22.9 (10.1)			18.2 (3.3)		
Duration (years)	10.4 (10.9)			4.9 (4.6)		
CPZeq (mg/day)	596.2 (556.2)			495.8 (541.6)		
PANSS positive	21.0 (6.3)			18.3 (6.3)		
PANSS negative	23.1 (7.5)			20.1 (6.4)		
PANSS general	50.0 (13.9)			45.8 (13.6)		
PANSS total	94.1 (26.2)			84.1 (25.5)		

Data are shown mean (standard deviation). CPZeq: chlorpromazine equivalent of total antipsychotics.
IQ: Intelligence Quotient, PANSS: Positive and Negative Symptom Scale.
doi:10.1371/journal.pone.0104619.t001

sequence was acquired with a 3D-spoiled GRASS sequence with magnetization transfer contrast: TR/TE = 38.4/2.4 ms, FA = 20 degrees, matrix size 480×320 in axial plane, FOV = 220 mm, and acquisition time = 3 min 25 s. A 40-mm slab thickness was used and images were reconstructed 40 slices with a slice thickness of 2 mm with in-slice zero-fill interpolation (ZIP2). We also obtained axial T2-weighted images of the whole brain to exclude coexisting disorders and any abnormal findings that might influence the signals for the SNc or LC. The T2-weighted image parameters are as follows: TR/TE = 4500/88 ms, FOV = 220 mm, Matrix = 512×256, 24 slices with slice thickness 5 mm, and 6 mm slice interval.

Data analysis

We measured the signal intensity of the SNc, midbrain tegmentum, LC, and pons. The region of interest (ROI) for the SNc was traced manually around the high signal area on two consecutive axial slices and ellipse ROI was set at midbrain tegmentum in the same slice (Figure 1B). An ellipse ROI for the LC and pons were indicated on three consecutive slices. The average and maximum signal intensities (MaxSR) and area were measured for each ROI. The measurements were performed by a blinded author. We calculated the contrast ratio (CR) of the SNc (CR_{SN}) and LC (CR_{LC}) using the following equations: $CR_{SN} = (S_{SN} - S_{TM})/S_{TM}$, $CR_{LC} = (S_{LC} - S_P)/S_P$. In these equations, S_{SN} and S_{TM} are the signal intensities for the SNc and midbrain tegmentum, respectively, and S_{LC} and S_P are the signal intensities of the LC and pons, respectively.

To reduce the effects of age-related changes in the CR_{SN} and CR_{LC}, we selected a subset of subjects who were under 30 years of age (n = 24 for schizophrenia, n = 29 for healthy controls) and compared their ROI values.

Statistical analyses were performed using unpaired *t*-tests to determine the differences between patients with schizophrenia and healthy controls.

Table 2. Neuromelanin imaging characteristics of patients with schizophrenia and healthy controls.

	Schizophrenia	controls	Schizophrenia	controls	Schizophrenia	controls
	all age n = 52	**all age n = 52**	**<30 years n = 24**	**<30 years n = 29**	**≥30 year n = 28**	**≥30 year n = 23**
CR_{SN} (%)	10.89±2.37*	9.60±2.36	10.51±2.11$	8.85±1.95	11.22±2.80	10.55±2.51
CR_{LC} (%)	14.21±3.5	13.44±3.37	13.73±3.37	13.15±3.88	14.63±3.56	13.79±2.69
Area-SNc (mm^2)	160.1±24.1	162.2±21.6	155.4±16.9	164.8±24.7	164.2±28.1	158.9±17.1
Area-LC (mm^2)	10.84±2.46	11.42±2.27	10.79±1.93	11.67±2.57	10.89±2.82	11.09±1.86
MaxSR SNc	1.32±0.04*	1.30±0.04	1.30±0.03*	1.28±0.03	1.33±0.04	1.32±0.04
MaxSR LC	1.28±0.05	1.27±0.05	1.27±0.05	1.28±0.06	1.29±0.05	1.27±0.04

SR, signal ratio; SNc, substantia nigra; LC, locus coeruleus; CR_{SN}, contrast ratio of SNc; CR_{LC}, contrast ratio of LC;
MaxSR, maximum signal intensity.
Data are presented as mean ± standard deviation.
*p<0.05 compared to controls,
$p<0.005 compared to controls.
doi:10.1371/journal.pone.0104619.t002

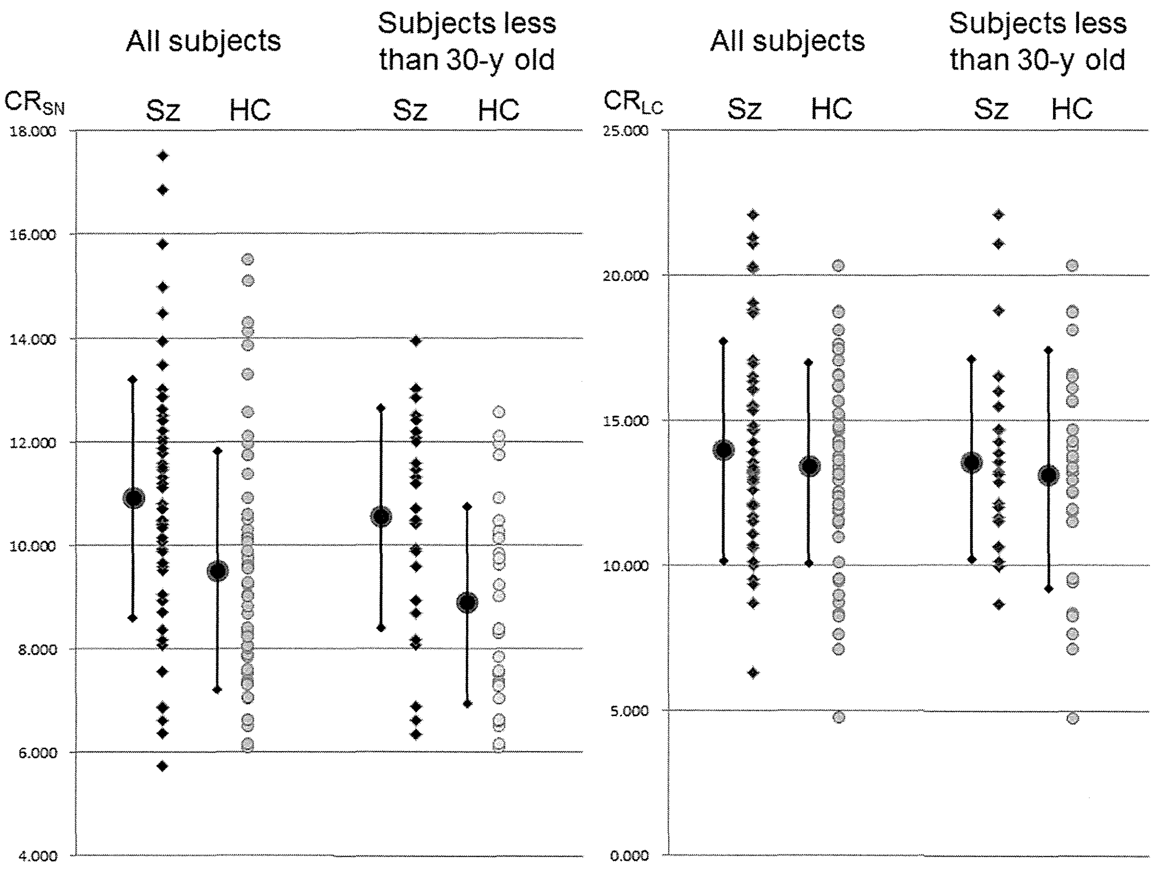

Figure 2. CR_{SN} and CR_{LC} for patients with schizophrenia and healthy controls. The left graph plots data for all subjects. The right graph plots data for selected patients under 30 years of age. The dots and bar show mean ± standard deviation. The patients showed a significantly higher CR_{SN}, but the variation in each group was large. The dispersion of data is small to select the young patients. There was no significant difference about CR_{LC} between the patients and healthy controls.
doi:10.1371/journal.pone.0104619.g002

We calculated the correlation between age and CR_{SN} or CR_{LC} for patients with schizophrenia and healthy controls. To elucidate the medication effects for the contrast ratio, the correlation between the chlorpromazine (CPZ) equivalents and CR_{SN} or CR_{LC} was analyzed.

Results

Table 1 presents the characteristics and clinical symptoms of patients and healthy controls. Compared to the patients, healthy controls had more years of education and higher IQs.

The SNc and LC were readily identified by high signal intensity areas in the posterior part of the cerebral peduncle and at the upper pontine tegmentum in both patients and healthy controls (Figure 1). Table 2 summarizes the mean signal intensities of each ROI. Our quantitative analysis showed that the CR_{SN} values and MaxSR SNc were significantly higher in patients with schizophrenia than in healthy controls (CR_{SN}: 10.89±2.37 vs. 9.6±2.36; $p<0.01$; Figure 2; MaxSR SNc: 1.32±0.04 vs. 1.30±0.04; $p<0.05$). No difference was observed in the CR_{LC} values between the patients and healthy controls (14.21±3.5 vs. 13.44±3.37; $p=0.25$; Figure 2). There was no difference the areas of the SNc and LC between schizophrenia and healthy controls.

In the subset of subjects that were under the age of 30, CR_{SN} values were significantly higher in patients with schizophrenia than in healthy controls (10.51±2.11 vs. 8.85±1.95; $p<0.005$; Figure 2). There was no significant difference for the subset of subjects over 30 years old.

There is weak correlation between age and CR_{SN} ($R=0.325$, $p=0.019$) for healthy controls and ($R=0.263$, $p=0.053$) for schizophrenia. There is no correlation between age and CR_{LC} ($R=-0.008$, $p=0.95$) for healthy controls and ($R=0.196$, $p=0.164$) for schizophrenia. The CPZ equivalent and CR_{SN} showed weak correlation ($R=0.353$, $p=0.010$) and there is no correlation between CPZ equivalent and CR_{LC} ($R=0.023$, $p=0.870$) for patients with schizophrenia.

Discussion

Our results demonstrate the excessive levels of dopamine products in the SNc of living patients with schizophrenia and this supports the dopamine hypothesis for schizophrenia. Recently, Howers et al [17] reported the same results using a post-mortem study, which revealed that tyrosine hydroxylase staining scores were significantly greater in the schizophrenia group at substantia nigra compared to in healthy controls and in vivo imaging using PET which showed that elevated dopamine synthesis was seen in the nigral dorpamine neurons in schizophrenia.

It has been suggested that dopamine dysfunction plays an important role in the pathogenesis of schizophrenia. This hypothesis is supported by evidence provided by numerous observations and studies. For example, the stimulants amphetamine and cocaine, which increase dopamine levels in the brain, can cause symptoms resembling those for psychosis [18]. Patients with Parkinson's disease who have been treated with levodopa, a dopamine-enhancing compound, can experience psychotic adverse effects mimicking the symptoms of schizophrenia [19]. Antipsychotic drugs such as chlorpromazine, however, can antagonize dopamine D2 receptor binding and reduce the positive symptoms of psychosis [20]. Lots of in vivo studies have used PET techniques that examine receptor imaging or dopamine synthesis in order to evaluate the dopamine system in patients with schizophrenia. Dopamine D2 receptors were upregulated in patients with schizophrenia [21] and increased striatal dopamine synthesis occurs in schizophrenia [3]. However, because of low-resolution of PET, many studies evaluated at striatum and cerebral cortex.

It has been reported that T1-weighted MRI with 3T can indicate T1-shortening tissues containing neuromelanin at SNc and LC [4,5]. This technique is widely used to investigate neuromelanin signal and volume loss in the SNc of patients with Parkinson's disease [6–9,22]. We are aware of only two previous reports on neuromelanin imaging in patients with schizophrenia. Shibata et al [11] described signal changes in the SNc and LC among patients with schizophrenia, depression and controls. However, the CR_{SN} values were higher in patients with schizophrenia ($n = 20$; 22.6±5.6: mean ± standard deviation (SD)) than in those with depression ($n = 18$; 19.2±4.7), as well as controls ($n = 34$; 19.6±3.8; one-way ANOVA, $p = 0.037$). However, a post hoc Tukey's test indicated no significant difference among schizophrenia and controls.

Sasaki et al [12] reported the CR_{SN} values were higher in patients with schizophrenia ($n = 23$; 22.6±5.1) than those with depression ($n = 23$; 19.0±4.3) and controls ($n = 23$; 20.5±3.4). A post hoc test confirmed a significant difference between patients with schizophrenia and those with depression, but not between patients with schizophrenia and controls.

These two previous reports indicate the CR_{SN} in patients with schizophrenia is higher than that in controls, but this was not statistically significant due to a small sample size and large variations. We performed a similar comparison in our study using a lager patient group (52 patients) and observed a significant difference. The mean CR_{SN} was significantly higher in patients with schizophrenia than in healthy controls, but the CR_{SN} values showed large variations with overlap between patients and healthy controls (Figure 2). It is reported that neuromelanin levels in the SNc can increase with age using post-mortem histrogical examination [23,24] and also neuro-melanin MRI [23,25]. The age range in our study was very broad, ranging from 17 to 69 years. To reduce age-related changes, we selected subjects younger than 30 years. Between these groups, the CR_{SN} value showed small variations, and the difference between patients and healthy controls was more prominent (Figure 2).

The absolute value of CR_{SN} observed in our study differed from those in two previous reports, which likely resulted from differences of the reference ROIs and MR sequence. We used a reference ROI located in the midbrain tegmentum, whereas previous reports used the decussation of the superior cerebellar peduncle. We use 3D-SPGR sequence to obtain T1-weighted image and previous reports performed a 2D-fast spin echo sequence. 3D acquisition is superior to obtain high signal to noise ratio image in less time. We showed significant difference using short time neuromelanin imaging and this was of great advantage to exam the schizophrenic patients who were sometimes difficult to hold steady head position for long examination time in MR unit.

There are several limitations to our study. First, we included all patients examined with neuromelanin MRI from April to November 2012. Many of these patients were under treatment with antipsychotic drugs. Our results showed that there is a weak correlation between CPZ equivalent and CR_{SN}, therefor these drugs have the potential to influence neuromelanin levels. The number of participants in this study was not enough to perform subgroup analysis and further study is needed to select first episode medication-naive patients to exclude the drug effect. Second, we could not evaluate the ventral tegmental area (VTA), which is the origin of the dopaminergic cell bodies of the mesolimbic-cortical dopaminergic system, because of the difficulty in detection the border of the VTA by neuromelanin-MRI. Third, the years of education and IQ were significantly higher in healthy controls than in patients with schizophrenia. Schizophrenia is characterized by general intellectual deficits [26,27]. The estimated premorbid IQ difference between schizophrenia and normal controls is smaller compared to that of full scale IQ, but the difference is statistically significant [28,29]. Fourth, we used 3D-SPGR imaging for neuromelanin MRI and the acquisition time was 3 min 25 s. Our acquisition time is shorter than that used for 2D-fast spin echo sequences in previous studies [4,5,11,12,30] and this short acquisition might make lower signal to noise ratio and large signal variability.

In conclusion, neuromelanin MRI revealed increased signal intensity in the SNc of patients with schizophrenia. This finding indicates the presence of an excessive level of dopamine products in the SNc of these patients. Therefore, neuromelanin imaging has the potential to be useful for accurate diagnosis of schizophrenia and to serve as a surrogate marker for medication.

Author Contributions

Conceived and designed the experiments: YW NT. Performed the experiments: YW HT AT YK MN RH HY M. Fujimoto. Analyzed the data: YW M. Fukunaga. Contributed reagents/materials/analysis tools: YW M. Fukunaga. Wrote the paper: YW.

References

1. Heinz A, Schlagenhauf F (2010) Dopaminergic dysfunction in schizophrenia: salience attribution revisited. Schizophr Bull 36: 472–485.
2. Abi-Dargham A, Rodenhiser J, Printz D, Zea-Ponce Y, Gil R, et al. (2000) Increased baseline occupancy of D2 receptors by dopamine in schizophrenia. Proc Natl Acad Sci U S A 97: 8104–8109.
3. Hietala J, Syvalahti E, Vuorio K, Rakkolainen V, Bergman J, et al. (1995) Presynaptic dopamine function in striatum of neuroleptic-naive schizophrenic patients. Lancet 346: 1130–1131.
4. Sasaki M, Shibata E, Tohyama K, Takahashi J, Otsuka K, et al. (2006) Neuromelanin magnetic resonance imaging of locus ceruleus and substantia nigra in Parkinson's disease. Neuroreport 17: 1215–1218.
5. Sasaki M, Shibata E, Tohyama K, Kudo K, Endoh J, et al. (2008) Monoamine neurons in the human brain stem: anatomy, magnetic resonance imaging findings, and clinical implications. Neuroreport 19: 1649–1654.
6. Kashihara K, Shinya T, Higaki F (2011) Neuromelanin magnetic resonance imaging of nigral volume loss in patients with Parkinson's disease. J Clin Neurosci 18: 1093–1096.
7. Schwarz ST, Rittman T, Gontu V, Morgan PS, Bajaj N, et al. (2011) T1-weighted MRI shows stage-dependent substantia nigra signal loss in Parkinson's disease. Mov Disord 26: 1633–1638.
8. Lehericy S, Sharman MA, Dos Santos CL, Paquin R, Gallea C (2012) Magnetic resonance imaging of the substantia nigra in Parkinson's disease. Mov Disord 27: 822–830.
9. Matsuura K, Maeda M, Yata K, Ichiba Y, Yamaguchi T, et al. (2013) Neuromelanin magnetic resonance imaging in Parkinson's disease and multiple system atrophy. Eur Neurol 70: 70–77.
10. Ohtsuka C, Sasaki M, Konno K, Koide M, Kato K, et al. (2013) Changes in substantia nigra and locus coeruleus in patients with early-stage Parkinson's disease using neuromelanin-sensitive MR imaging. Neurosci Lett 541: 93–98.

11. Shibata E, Sasaki M, Tohyama K, Otsuka K, Endoh J, et al. (2008) Use of neuromelanin-sensitive MRI to distinguish schizophrenic and depressive patients and healthy individuals based on signal alterations in the substantia nigra and locus ceruleus. Biol Psychiatry 64: 401–406.
12. Sasaki M, Shibata E, Ohtsuka K, Endoh J, Kudo K, et al. (2010) Visual discrimination among patients with depression and schizophrenia and healthy individuals using semiquantitative color-coded fast spin-echo T1-weighted magnetic resonance imaging. Neuroradiology 52: 83–89.
13. Kay SR, Fiszbein A, Opler LA (1987) The positive and negative syndrome scale (PANSS) for schizophrenia. Schizophr Bull 13: 261–276.
14. Committee JW-IP (2006) Japanese Wechsler Adult Intelegence Scale Third Edition. Tokyo: Nihon Bunka Kagakusha.
15. Ota T, Iida J, Sawada M, Suehiro Y, Kishimoto N, et al. (2013) Comparison of pervasive developmental disorder and schizophrenia by the Japanese version of the National Adult Reading Test. Int J Psychiatry Clin Pract 17: 10–15.
16. Matsuoka K, Uno M, Kasai K, Koyama K, Kim Y (2006) Estimation of premorbid IQ in individuals with Alzheimer's disease using Japanese ideographic script (Kanji) compound words: Japanese version of National Adult Reading Test. Psychiatry Clin Neurosci 60: 332–339.
17. Howes OD, Williams M, Ibrahim K, Leung G, Egerton A, et al. (2013) Midbrain dopamine function in schizophrenia and depression: a post-mortem and positron emission tomographic imaging study. Brain 136: 3242–3251.
18. Gururajan A, Manning EE, Klug M, van den Buuse M (2012) Drugs of abuse and increased risk of psychosis development. Aust N Z J Psychiatry 46: 1120–1135.
19. Zahodne LB, Fernandez HH (2008) Pathophysiology and treatment of psychosis in Parkinson's disease: a review. Drugs Aging 25: 665–682.
20. Seeman P (2010) Dopamine D2 receptors as treatment targets in schizophrenia. Clin Schizophr Relat Psychoses 4: 56–73.
21. Wong DF, Wagner HN Jr, Tune LE, Dannals RF, Pearlson GD, et al. (1986) Positron emission tomography reveals elevated D2 dopamine receptors in drug-naive schizophrenics. Science 234: 1558–1563.
22. Ogisu K, Kudo K, Sasaki M, Sakushima K, Yabe I, et al. (2013) 3D neuromelanin-sensitive magnetic resonance imaging with semi-automated volume measurement of the substantia nigra pars compacta for diagnosis of Parkinson's disease. Neuroradiology 55: 719–724.
23. Zucca FA, Bellei C, Giannelli S, Terreni MR, Gallorini M, et al. (2006) Neuromelanin and iron in human locus coeruleus and substantia nigra during aging: consequences for neuronal vulnerability. J Neural Transm 113: 757–767.
24. Mann DM, Yates PO (1974) Lipoprotein pigments–their relationship to ageing in the human nervous system. II. The melanin content of pigmented nerve cells. Brain 97: 489–498.
25. Tanaka M, Aihara Y, Ikeda S, Aihara Y (2011) [Neuromelanin-related contrast in the substantia nigra semiquantitatively evaluated by magnetic resonance imaging at 3T: comparison between normal aging and Parkinson disease]. Rinsho Shinkeigaku 51: 14–20.
26. Bilder RM, Reiter G, Bates J, Lencz T, Szeszko P, et al. (2006) Cognitive development in schizophrenia: follow-back from the first episode. J Clin Exp Neuropsychol 28: 270–282.
27. Keefe RS, Eesley CE, Poe MP (2005) Defining a cognitive function decrement in schizophrenia. Biol Psychiatry 57: 688–691.
28. Fujino H, Sumiyoshi C, Sumiyoshi T, Yasuda Y, Yamamori H, et al. (2014) Performance on the Wechsler Adult Intelligence Scale-III in Japanese patients with schizophrenia. Psychiatry Clin Neurosci.
29. Woodberry KA, Giuliano AJ, Seidman LJ (2008) Premorbid IQ in schizophrenia: a meta-analytic review. Am J Psychiatry 165: 579–587.
30. Shibata E, Sasaki M, Tohyama K, Kanbara Y, Otsuka K, et al. (2006) Age-related changes in locus ceruleus on neuromelanin magnetic resonance imaging at 3 Tesla. Magn Reson Med Sci 5: 197–200.

Jpn J Radiol (2015) 33:26–32
DOI 10.1007/s11604-014-0376-z

ORIGINAL ARTICLE

Model-based iterative reconstruction for detection of subtle hypoattenuation in early cerebral infarction: a phantom study

Mitsuo Nishizawa · Hisashi Tanaka · Yoshiyuki Watanabe · Yuuki Kunitomi · Akio Tsukabe · Noriyuki Tomiyama

Received: 5 October 2014 / Accepted: 12 November 2014 / Published online: 26 November 2014

Abstract

Purpose Model-based iterative reconstruction (MBIR) was recently shown to enable dose reduction in computed tomography (CT). The detectability of low-contrast lesions was assessed on CT images reconstructed with MBIR compared with the conventional filtered back-projection (FBP) method.

Materials and methods A phantom simulating brain gray matter containing small lesions mimicking early cerebral infarctions was scanned at tube currents of 50, 100, 200, and 400 mA. Images were reconstructed by use of both methods. Round regions were cropped from the reconstructed images, half with a lesion, the other half without. Eight radiologists reviewed the images and scored the certainty of lesion detection on a 5-point scale. Overall performance was analyzed by use of a receiver operating characteristic curve.

Results For the tube currents investigated, the analysis showed that the mean areas under the curves for the reviewers were 0.65, 0.70, 0.82, and 0.83 for FBP and 0.70, 0.76, 0.78, and 0.90 for MBIR. For each current, there was no significant difference between the areas under the curves for the different reconstruction methods ($p = 0.32$, 0.24, 0.49, and 0.17).

Conclusion For the small, low-contrast lesions in the phantom model used in this study, no significant difference between detectability was observed for MBIR and FBP.

Keywords Model-based iterative reconstruction · Computed tomography · Dose reduction · Lesion detectability · Noise power spectrum

M. Nishizawa · H. Tanaka · Y. Watanabe · Y. Kunitomi · A. Tsukabe · N. Tomiyama
Department of Diagnostic and Interventional Radiology, Osaka University Graduate School of Medicine, 2-2, Yamadaoka, Suita, Osaka 565-0871, Japan

M. Nishizawa (✉)
Department of Diagnostic Radiology, Osaka Medical College, 2-7, Daigaku-machi, Takatsuki, Osaka 569-8686, Japan
e-mail: m-nishizawa@radiol.med.osaka-u.ac.jp; mnishizawa@poh.osaka-med.ac.jp

Introduction

Use of computed tomography (CT) in clinical examinations has been rapidly increasing in recent years. Because of public concern that increased radiation exposure has recently escalated the potential risk of cancer [1], dose-reduction techniques have been pursued for CT. However, increased image noise in lower radiation-dose CT may result in diagnostic inaccuracy. A currently widely used reconstruction algorithm, filtered back projection (FBP), is unable to consistently generate diagnostic-quality images for reduced X-ray tube currents [2–4].

In recent years, vendors have developed new iterative reconstruction methods [5] which have been reported to provide better image quality than FBP [6]. Among these, model-based iterative reconstruction (MBIR), recently developed as the Veo system by GE Healthcare (Waukesha, WI, USA), is a full iterative reconstruction algorithm that models both the photon statistics in X-ray attenuation and the system optics [7, 8]. It results in marked noise reduction and potentially reduces radiation dose. MBIR currently requires much reconstruction time, for example 1 h or more, because of its computationally intensive nature. However, progress in computer software and hardware technology is expected to reduce the time required for reconstruction, so full iterative reconstruction methods, for example MBIR, can become a mainstay of CT reconstruction.

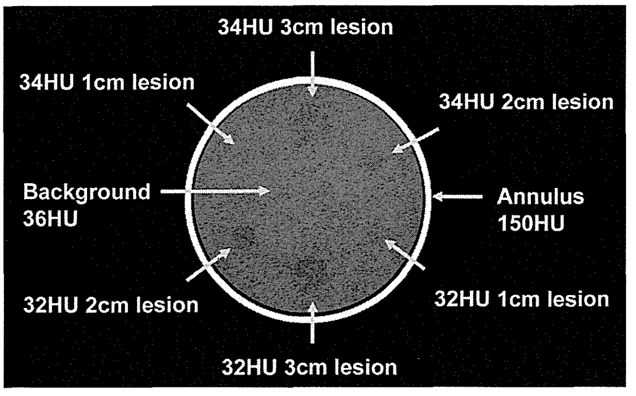

Fig. 1 Transverse CT image of the phantom (FBP; 400 mA; 5 mm thickness). Six hypoattenuation lesions in the phantom and the annulus simulating the skull are indicated by *arrows*

Although, in patient and phantom studies, MBIR has been reported to be superior to FBP [9–20], few studies of application of new iterative reconstruction methods to the cranial region have been reported [21–26], and these include just one report for MBIR on CT angiography [13]. As far as we are aware, the efficacy of MBIR in cases of cerebral infarction, a major cause of mortality and morbidity, has not been reported. The diagnostic effectiveness of low radiation doses should be investigated, because dose reduction in cranial CT can lead to a risk of missing subtle lesions as early cerebral infarctions. Therefore, the purpose of this study was to assess the detectability of low-contrast lesions on CT images at different tube currents reconstructed with MBIR compared with FBP. A phantom was used to simulate cerebral infarctions.

Materials and methods

Low-contrast phantom

A cylindrical phantom (Kyoto Kagaku, Kyoto, Japan) was used to simulate the typical contrast of both early cytotoxic brain edema and cerebral infarction on brain CT images (Fig. 1) [27]. The phantom was 18 cm in diameter and was made of acrylic resin, resulting in a nominal attenuation of 36 Hounsfield units (HU) at a scanning tube voltage of 120 kVp, simulating brain gray matter. The phantom had six "cerebral infarctions" consisting of two sets of acrylic resin spheres 3, 2, and 1 cm in diameter; the nominal attenuation of each set was adjusted to 34 and 32 HU, corresponding to CT hypoattenuation values of early ischemic brain damage and infarction, respectively. In addition, an annulus simulating a skull was attached to the exterior of the phantom. The annulus was 1 cm in thickness and was made of epoxy resin, resulting in a nominal attenuation of 500 HU at 120 kVp. The k-edge of the phantom was 15 keV, which was less than the conventional radiographic spectra produced by the CT scanner during normal operation.

Data acquisition and image reconstruction

All examinations were acquired by use of a 64-slice multidetector CT (GE Discovery 750 HD; GE Healthcare). The phantom was placed at the edge of the patient table by use of an attachment provided as an optional accessory. It was then carefully positioned such that the center axis of the phantom was at the isocenter of the scanner. All measurements were performed in axial (non-helical) mode. The phantom was scanned by using a detector configuration of 64 rows $\times$ 0.625 mm; acquisition was performed at a tube voltage of 120 kVp with tube currents of 50, 100, 200, and 400 mA and a rotation time of 0.8 s. Identical scans were repeated three times to ensure that the acquired images were not affected by variance in detector noise during each scan.

All images were reconstructed with 0.625-mm-thick axial slices. From the same raw image data, images were reconstructed with the FBP and MBIR algorithms. Because of limitations of the system, only 0.625-mm-thick images can be reconstructed directly by use of MBIR. Images 5 mm thick were constructed by adding eight serial 0.625-mm-thick reconstructed images by use of MATLAB R2007a (Mathworks, Natick, MA, USA). This procedure was performed because clinical CT images for diagnosis of cerebral infarction are usually acquired with a slice thickness of 5 mm at our institution.

Measurement of background image noise

The standard deviation (SD) of the signal was measured in four square regions in the central portion of the phantom, which contained no simulated lesions, for each imaging condition. These were considered as the background CT image noise.

Preparation of images for visual evaluation

Each reconstructed image contained six hypoattenuating lesions. For evaluation of the visual detectability of hypoattenuating lesions, eight round regions 4.6 cm in diameter were cropped from one 5-mm-thick image: two with a lesion 1 cm in diameter, two with a lesion 2 cm in diameter, and four with no lesions. Lesions 3 cm in diameter were excluded from further evaluation, because these lesions are easy to detect with both reconstruction methods at the

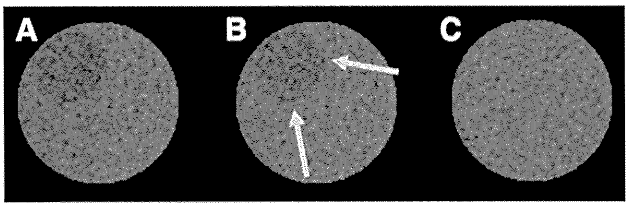

Fig. 2 Examples of the small, round, and cropped regions used for visual evaluation. **a** Contains a lesion of 32 HU. **b** is an image identical with (**a**) with *arrows* that indicate the lesion. **c** Contains no lesion

lowest tube current of 50 mA. Each round region with a lesion was cropped such that the lesion was situated off-center in the resulting round image (Fig. 2). These round images were then randomly flipped vertically and/or horizontally. The purpose of this procedure was to prevent the readers from having prior knowledge of the lesion location in each image.

We obtained 192 round images (3 scans × 4 currents × 2 reconstructions × 8 round images) per 5 mm slice for visual inspection in this way, half with a lesion, and the other half without lesions. The order of images was then randomized.

Visual evaluation

Eight radiologists independently reviewed the resulting image pieces (small round regions) on a monitor screen with a fixed window level of 35 HU and window width of 100 HU. They were informed that each image piece contained one lesion or no lesion. Information about lesion incidence was not provided. The certainty of lesion detection was scored on a 5-point scale, representing definitely absent, probably absent, equivocal, probably present, and definitely present.

Statistical analysis

Overall performance in the visual evaluations was investigated by sensitivity analysis, with a receiver operating characteristic (ROC) curve and area under the curve (AUC) computations for the different tube currents and reconstruction methods.

Binormal ROC curves were estimated by use of Dorfman–Berbaum–Metz multiple readers and a multiple cases algorithm (DBM MRMC 2.33) [28, 29]. A contaminated binormal model was used for curve fitting, and DBM analysis was performed for random readers and random cases.

A paired t test was used to compare the SDs of the background image noise.

All values are expressed as the mean ± standard error of the mean.

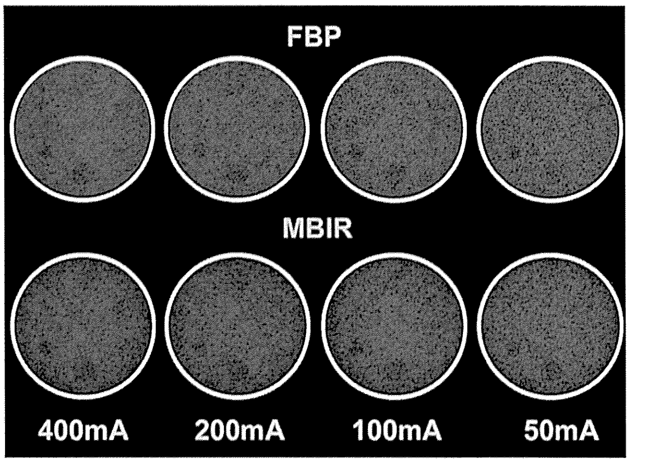

Fig. 3 Phantom images reconstructed by use of FBP and MBIR for tube currents of 50, 100, 200, and 400 mA

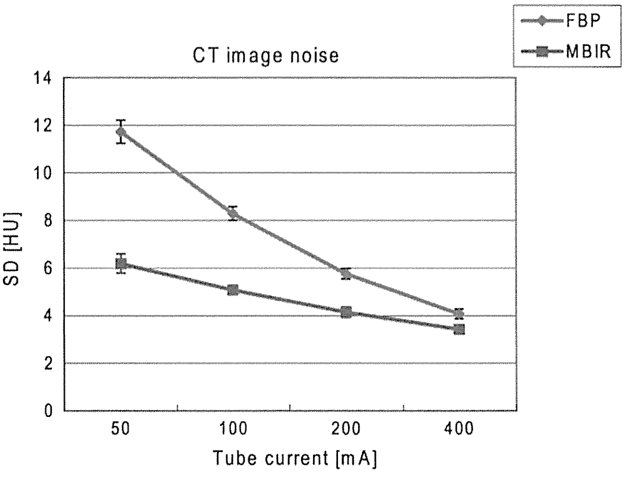

Fig. 4 Image noise (SD) at different tube currents for FBP and MBIR. *Vertical error bars* indicate the standard deviation

Analysis of the noise power spectrum

The noise power spectrum (NPS) of the CT image was analyzed by use of both reconstruction methods. Images were acquired with a Catphan 500 (Phantom Laboratory, Salem, NY, USA) with image uniformity module (CTP 486), by use of the same CT scanner with a detector configuration of 64 rows × 0.625 mm, a tube voltage of 120 kVp, tube currents of 50 and 400 mA, a rotation time of 0.8 s, and a pitch of 0.531:1 in helical mode. Images were reconstructed by use of FBP and MBIR. The one-dimensional (1D) NPS were analyzed by use of a synthesized slit technique [30, 31] wherein five non-overlapping slits, each 30 × 256 pixels, were selected. The 1D Fourier transform was calculated in the direction of the 256 pixel side for each slit. The NPS of the image was obtained by averaging the power spectra of the five slits.

Results

Reconstructed images

Phantom images reconstructed by use of FBP and MBIR for different tube currents are shown in Fig. 3.

Background CT image noise

CT image noise was measured by calculating the SD of the background signal in areas containing no lesion. The measured SDs were 11.73 ± 0.14, 8.29 ± 0.08, 4.96 ± 0.06, and 4.08 ± 0.06 HU for FBP, and 6.19 ± 0.12, 5.08 ± 0.06, 4.15 ± 0.07, and 3.43 ± 0.05 HU for MBIR, for tube currents of 50, 100, 200, and 400 mA, respectively (Fig. 4). The SD of the MBIR-reconstructed images was significantly smaller than that of the FBP images for each tube current ($p < 0.001$).

Image noise was less for higher tube currents. The image noise from the MBIR reconstructed image was lower than that from the FBP reconstructed image under corresponding imaging conditions. The difference between the image noise for these methods was larger at lower tube currents.

Visual evaluation of the low-contrast phantom

The ROC analysis showed that the mean AUCs for the eight reviewers were 0.65 ± 0.07, 0.70 ± 0.05, 0.82 ± 0.08, and 0.83 ± 0.05 for FBP and 0.70 ± 0.07, 0.76 ± 0.06, 0.78 ± 0.06, and 0.90 ± 0.04 for MBIR, for tube currents of 50, 100, 200, and 400 mA, respectively (Fig. 5).

Smaller AUCs were associated with lower tube currents for both FBP and MBIR. For each tube current there was no significant difference between the AUCs for FBP and MBIR ($p = 0.32$, 0.24, 0.49, and 0.17, for tube currents of 50, 100, 200, and 400 mA, respectively).

Noise power spectrum

The NPS for tube currents of 50 and 400 mA are shown in Figs. 6 and 7, respectively, for each reconstruction method.

The overall amount of noise for MBIR was much less than that for FBP. The difference between the noise components for these methods was smaller at low spatial frequencies (for example, at 0.1 cycles/mm) than at high spatial frequencies (for example, at 1.1 cycles/mm) for both tube currents.

Discussion

Iterative reconstruction methods are promoted as enabling substantial reductions in radiation doses without impairing image quality. However, most reported investigations have focused on assessment of visual impressions of image quality or technical indices, for example image noise, contrast-to-noise ratio, and spatial resolution. The diagnostic effectiveness of iterative reconstruction cannot be assessed on the basis of such visual impressions or technical indices alone. In this study, not just visual impressions but diagnostic performance was measured. The detectability of low-contrast lesions was not improved by use of MBIR in our experiment, although the CT image noise (SD) was lower with MBIR than with FBP at low tube currents.

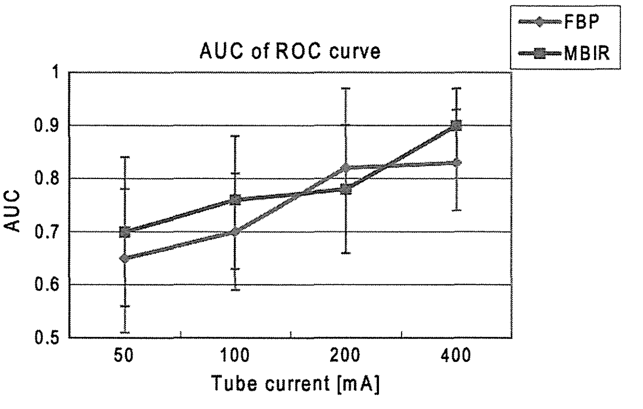

Fig. 5 Area under the curve (AUC) for different tube currents for FBP and MBIR. The AUC shows the diagnostic performance. The *vertical error bars* indicate 95 %-confidence intervals

Recently, low-contrast lesion detectability by use of iterative reconstruction has been evaluated by a few groups. There are, however, still arguments regarding the efficacy of iterative reconstruction for improvement of detection of low-contrast objects. Some have reported that sinogram affirmed iterative reconstruction (SAFIRE; Siemens Medical Solutions, Forchheim, Germany) or adaptive iterative dose reduction 3-D (AIDR 3-D; Toshiba Medical Systems, Tokyo, Japan) did not improve low-contrast detectability when low doses of radiation were used with phantoms simulating liver tumors [32, 33]. Another study, using a pediatric trunk phantom, compared MBIR, adaptive statistical iterative reconstruction (ASIR; GE Healthcare), and iDose[4] (Philips Healthcare, Best, The Netherlands) with FBP, and reported that only MBIR improved low-contrast lesion detection at low radiation doses [34]. The reasons for the discrepancy between their result and ours for MBIR may be multifactorial. Their study used a tube voltage of 80 kVp, and the difference between the CT values for lesion and background was 10 HU, which was larger than that used in our study.

Although several patient studies have been conducted on MBIR investigation lesion detection, they did not focus on low-contrast lesions [11, 17, 18].

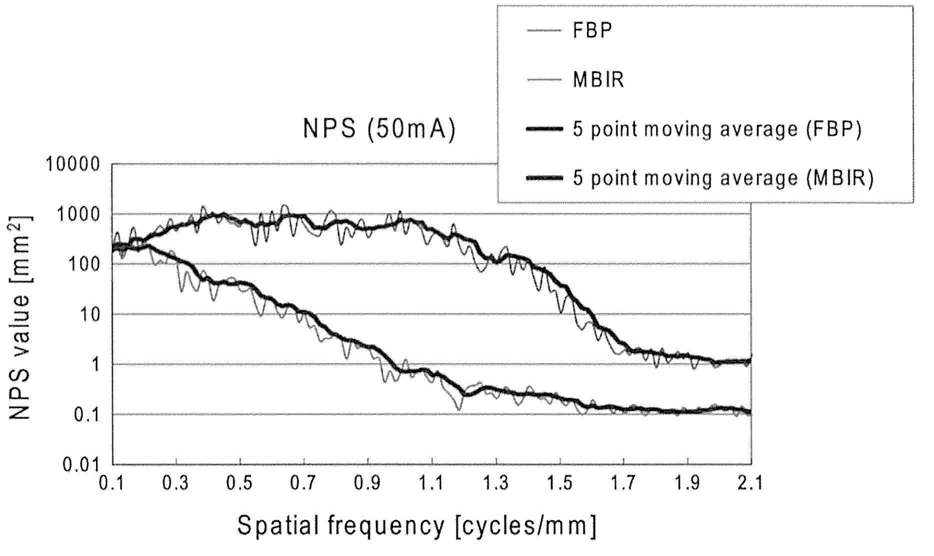

Fig. 6 The noise power spectrum (NPS) for a tube current of 50 mA for FBP and MBIR

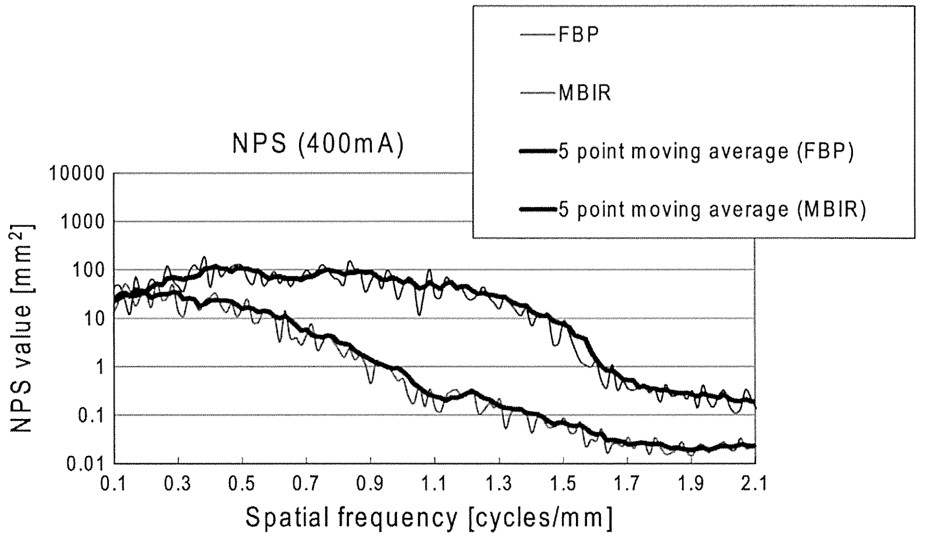

Fig. 7 NPS at a tube current of 400 mA for FBP and MBIR

The reason there was no significant difference between the diagnostic performance of FBP and MBIR in the detection of low-contrast lesions in this study can be speculated as follows. According to signal detection theory [35–38], the signal-to-noise ratio (SNR) for a SKE-BKE (signal known exactly, background known exactly) detection task in a two-dimensional (2D) image is represented by:

$$\mathrm{SNR} = \frac{\iint \mathrm{d}f_x \mathrm{d}f_y \left| R(f_x,f_y) \right|^2}{\left[\iint \mathrm{d}f_x \mathrm{d}f_y S(f_x,f_y) \left| R(f_x,f_y) \right|^2 \right]^{1/2}}$$

where $R(f_x, f_y)$ is the 2D Fourier transform of the signal of the object to be detected and $S(f_x, f_y)$ is the 2D NPS of the background [36]. This shows that background noise affects detectability only in respect of the integral of the product of $S(f_x, f_y)\ |R(f_x, f_y)|^2$. In our study, objects to be detected were small circular regions, and $|R(f_x, f_y)|^2$ was very small for large values of f_x or f_y. In such cases, $S(f_x, f_y)$ for high spatial frequencies contributes little to the integral. Thus, the high-frequency component of the noise does not substantially affect detectability. The NPS analysis in this study showed that MBIR can reduce much of the high-frequency components of the noise, but less so for the low-frequency components (Figs. 6, 7). Low-frequency components of noise cannot be substantially reduced with MBIR, although the overall amount of noise is much lower with MBIR than with FBP at low tube currents. This could explain why the detectability of low-contrast objects was not improved with MBIR.

The clinical significance of this study is that MBIR may have little efficacy in radiation dose reduction when used for detection of early cerebral infarctions.

This study had several limitations. The phantom used simulates just three components of the head, namely the skull, normal brain parenchyma, and infarctions. The sulci, gyri, vessels, or other detailed structures were not considered. In addition, the contrast of the gray and white matter of the brain was also not simulated by the phantom. This limitation, however, does not seem to affect the results substantially, because the low-contrast lesions to be detected in this study were larger than the brain substructures.

Conclusions

For the small, low-contrast lesions in this phantom model, detectability by use of MBIR and FBP reconstruction methods was not significantly different. Thus dose reduction by use of MBIR in cranial CT must be limited to preserve diagnostic effectiveness in the detection of early cerebral infarctions.

Conflict of interest The authors declare that they have no conflict of interest.

References

1. Brenner DJ, Hall EJ. Computed tomography—an increasing source of radiation exposure. N Engl J Med. 2007;357(22):2277–84.
2. Pan X, Sidkey EY, Vannier M. Why do commercial CT scanners still employ traditional, filtered back-projection for image reconstruction? Inverse Prob. 2009;25:1–37.
3. Cohnen M, Fischer H, Hamacher J, Lins E, Kötter R, Mödder U. CT of the head by use of reduced current and kilovoltage: relationship between image quality and dose reduction. Am J Neuroradiol. 2000;21:1654–60.
4. Mullins ME, Lev MH, Bove P, O'Reilly CE, Saini S, Rhea JT, et al. Comparison of image quality between conventional and low-dose nonenhanced head CT. Am J Neuroradiol. 2004;25:533–8.
5. Willemink MJ, de Jong PA, Leiner T, de Heer LM, Nievelstein RA, Budde RP, et al. Iterative reconstruction techniques for computed tomography Part 1: technical principles. Eur Radiol. 2013;23:1623–31.
6. Willemink MJ, Leiner T, de Jong PA, de Heer LM, Nievelstein RA, Schilham AM, et al. Iterative reconstruction techniques for computed tomography part 2: initial results in dose reduction and image quality. Eur Radiol. 2013;23:1632–42.
7. Thibault JB, Sauer KD, Bouman CA, Hsieh J. A three-dimensional statistical approach to improved image quality for multislice helical CT. Med Phys. 2007;34:4526–44.
8. Yu Z, Thibault J-B, Bouman CA, Sauer KD, Hsieh J. Fast model-based X-ray CT reconstruction using spatially nonhomogeneous ICD optimization. IEEE Trans Image Process. 2010;20:161–75.
9. Scheffel H, Stolzmann P, Schlett CL, Engel LC, Major GP, Karolyi M, et al. Coronary artery plaques: cardiac CT with model-based and adaptive-statistical iterative reconstruction technique. Eur J Radiol. 2012;81:e363–9.
10. Katsura M, Matsuda I, Akahane M, Sato J, Akai H, Yasaka K, et al. Model-based iterative reconstruction technique for radiation dose reduction in chest CT: comparison with the adaptive statistical iterative reconstruction technique. Eur Radiol. 2012;22:1613–23.
11. Pickhardt PJ, Lubner MG, Kim DH, Tang J, Ruma JA, del Rio AM, et al. Abdominal CT with model-based iterative reconstruction (MBIR): initial results of a prospective trial comparing ultralow-dose with standard-dose imaging. Am J Roentgenol. 2012;199:1266–74.
12. Deak Z, Grimm JM, Treitl M, Geyer LL, Linsenmaier U, Korner M, et al. Filtered back projection, adaptive statistical iterative reconstruction, and a model-based iterative reconstruction in abdominal CT: an experimental clinical study. Radiology. 2013;266:197–206.
13. Machida H, Takeuchi H, Tanaka I, Fukui R, Shen Y, Ueno E, et al. Improved delineation of arteries in the posterior fossa of the brain by model-based iterative reconstruction in volume-rendered 3D CT angiography. Am J Neuroradiol. 2013;34:971–5.
14. Machida H, Tanaka I, Fukui R, Kita K, Shen Y, Ueno E, et al. Improved delineation of the anterior spinal artery with model-based iterative reconstruction in CT angiography: a clinical pilot study. Am J Roentgenol. 2013;200:442–6.
15. Vardhanabhuti V, Loader RJ, Mitchell GR, Riordan RD, Roobottom CA. Image quality assessment of standard- and low-dose chest CT using filtered back projection, adaptive statistical iterative reconstruction, and novel model-based iterative reconstruction algorithms. Am J Roentgenol. 2013;200:545–52.
16. Suzuki S, Machida H, Tanaka I, Ueno E. Vascular diameter measurement in CT angiography: comparison of model-based iterative reconstruction and standard filtered back projection algorithms in vitro. Am J Roentgenol. 2013;200:652–7.
17. Shuman WP, Green DE, Busey JM, Kolokythas O, Mitsumori LM, Koprowicz KM, et al. Model-based iterative reconstruction versus adaptive statistical iterative reconstruction and filtered back projection in liver 64-MDCT: focal lesion detection, lesion conspicuity, and image noise. Am J Roentgenol. 2013;200:1071–6.
18. Volders D, Bols A, Haspeslagh M, Coenegrachts K. Model-based iterative reconstruction and adaptive statistical iterative reconstruction techniques in abdominal ct: comparison of image quality in the detection of colorectal liver metastases. Radiology. 2013;269:469–74.
19. Nishida J, Kitagawa K, Nagata M, Yamazaki A, Nagasawa N, Sakuma H. Model-based iterative reconstruction for multi-detector row CT assessment of the Adamkiewicz artery. Radiology. 2014;270:282–91.
20. Smith EA, Dillman JR, Goodsitt MM, Christodoulou EG, Keshavarzi N, Strouse PJ. Model-based iterative reconstruction: effect on patient radiation dose and image quality in pediatric body CT. Radiology. 2014;270:526–34.
21. Korn A, Fenchel M, Bender B, Danz S, Hauser TK, Ketelsen D, et al. Iterative reconstruction in head CT: image quality of routine and low-dose protocols in comparison with standard filtered back-projection. Am J Neuroradiol. 2012;33:218–24.
22. Wu TH, Hung SC, Sun JY, Lin CJ, Lin CH, Chiu CF, et al. How far can the radiation dose be lowered in head CT with iterative reconstruction? Analysis of imaging quality and diagnostic accuracy. Eur Radiol. 2013;23:2612–21.
23. Vorona GA, Zuccoli G, Sutcavage T, Clayton BL, Ceschin RC, Panigrahy A. The use of adaptive statistical iterative reconstruction in pediatric head CT: a feasibility study. Am J Neuroradiol. 2013;34:205–11.
24. Rapalino O, Kamalian S, Kamalian S, Payabvash S, Souza LC, Zhang D, et al. Cranial CT with adaptive statistical iterative reconstruction: improved image quality with concomitant radiation dose reduction. Am J Neuroradiol. 2012;33:609–15.

25. Kilic K, Erbas G, Guryildirim M, Arac M, Ilgit E, Coskun B. Lowering the dose in head CT using adaptive statistical iterative reconstruction. AJNR Am J Neuroradiol. 2011;32:1578–82.
26. Ren Q, Dewan SK, Li M, Li J, Mao D, Wang Z, et al. Comparison of adaptive statistical iterative and filtered back projection reconstruction techniques in brain CT. Eur J Radiol. 2012;81:2597–601.
27. Tanaka C, Ueguchi T, Shimosegawa E, Sasaki N, Johkoh T, Nakamura H, et al. Effect of CT acquisition parameters in the detection of subtle hypoattenuation in acute cerebral infarction: a phantom study. Am J Neuroradiol. 2006;27:40–5.
28. Dorfman DD, Berbaum KS, Metz CE. Receiver operating characteristic rating analysis. Generalization to the population of readers and patients with the jackknife method. Invest Radiol. 1992;27:723–31.
29. Medical Image Perception Laboratory > Software > Receiver Operating Characteristic (ROC) > DBM MRMC. 2013. http://perception.radiology.uiowa.edu/Software/ReceiverOperatingCharacteristicROC/DBMMRMC/tabid/116/Default.aspx. Accessed 07 Oct 2013.
30. Siewerdsen JH, Antonuk LE, el-Mohri Y, Yorkston J, Huang W, Cunningham IA. Signal, noise power spectrum, and detective quantum efficiency of indirect-detection flat-panel imagers for diagnostic radiology. Med Phys. 1998;25:614–28.
31. Giger ML, Doi K, Metz CE. Investigation of basic imaging properties in digital radiography. 2. Noise wiener spectrum. Med Phys. 1984;11:797–805.
32. Baker ME, Dong F, Primak A, Obuchowski NA, Einstein D, Gandhi N, et al. Contrast-to-noise ratio and low-contrast object resolution on full- and low-dose MDCT: sAFIRE versus filtered back projection in a low-contrast object phantom and in the liver. Am J Roentgenol. 2012;199:8–18.
33. Schindera ST, Odedra D, Raza SA, Kim TK, Jang H-J, Szucs-Farkas Z, et al. Iterative reconstruction algorithm for CT: can radiation dose be decreased while low-contrast detectability is preserved? Radiology. 2013;269:511–8.
34. Mieville FA, Gudinchet F, Brunelle F, Bochud FO, Verdun FR. Iterative reconstruction methods in two different MDCT scanners: physical metrics and 4-alternative forced-choice detectability experiments–a phantom approach. Phys Med. 2013;29:99–110.
35. Wagner RF. Decision theory and the detail signal-to-noise ratio of otto schade. Photogr Sci Eng. 1978;22:1–6.
36. Hanson KM. Detectability in computed tomographic images. Med Phys. 1979;6:441–51.
37. Loo LN, Doi K, Metz CE. A comparison of physical image quality indices and observer performance in the radiographic detection of nylon beads. Phys Med Biol. 1984;29:837–56.
38. Barrett HH, Myers KJ. Foundations of image science. Wiley Intersci. 2004:801–1000.